EBioMedicine 55 (2020) 102750

Contents lists available at ScienceDirect

EBioMedicine

journal homepage: www.elsevier.com/locate/ebiom

Research paper

Motor transmission defects with sex differences in a new mouse model of mild spinal muscular atrophy

Marc-Olivier Deguise[a,b,c], Yves De Repentigny[a], Alexandra Tierney[a], Ariane Beauvais[a], Jean Michaud[d], Lucia Chehade[a,b,c], Mohamed Thabet[b], Brittany Paul[a,c], Aoife Reilly[a,b,c], Sabrina Gagnon[a], Jean-Marc Renaud[b,c], Rashmi Kothary[a,b,c,e,f,*]

[a] Regenerative Medicine Program, Ottawa Hospital Research Institute, 501 Smyth Road, Ottawa, Ontario K1H 8L6, Canada
[b] Department of Cellular and Molecular Medicine, University of Ottawa, Ottawa, Ontario K1H 8M5, Canada
[c] Centre for Neuromuscular Disease, University of Ottawa, Ottawa, Ontario K1H 8M5, Canada
[d] Department of Pathology and Laboratory Medicine, Faculty of Medicine, University of Ottawa, Ottawa, Ontario K1H 8M5, Canada
[e] Department of Biochemistry, Microbiology, and Immunology, Faculty of Medicine, University of Ottawa, Ottawa, Ontario K1H 8M5, Canada
[f] Department of Medicine, University of Ottawa, Ottawa, Ontario K1H 8M5, Canada

ARTICLE INFO

Article History:
Received 18 September 2019
Revised 25 February 2020
Accepted 19 March 2020
Available online xxx

Keywords:
Aging
SMN
Type IV
Electrophysiology
Sex difference
Non-neuronal defects

ABSTRACT

Background: Mouse models of mild spinal muscular atrophy (SMA) have been extremely challenging to generate. This paucity of model systems has limited our understanding of pathophysiological events in milder forms of the disease and of the effect of SMN depletion during aging.
Methods: A mild mouse model of SMA, termed $Smn^{2B/-}$;$SMN2^{+/-}$, was generated by crossing $Smn^{-/-}$;*SMN2* and $Smn^{2B/2B}$ mice. This new model was characterized using behavioral testing, histology, western blot, muscle-nerve electrophysiology as well as ultrasonography to study classical SMA features and extra-neuronal involvement.
Findings: $Smn^{2B/-}$;$SMN2^{+/-}$ mice have normal survival, mild but sustained motor weakness, denervation and neuronal/neuromuscular junction (NMJ) transmission defects, and neurogenic muscle atrophy that are more prominent in male mice. Increased centrally located nuclei, intrinsic contractile and relaxation muscle defects were also identified in both female and male mice, with some male predominance. There was an absence of extra-neuronal pathology.
Interpretation: The $Smn^{2B/-}$;$SMN2^{+/-}$ mouse provides a model of mild SMA, displaying some hallmark features including reduced weight, sustained motor weakness, electrophysiological transmission deficit, NMJ defects, and muscle atrophy. Early and prominent increase central nucleation and intrinsic electrophysiological deficits demonstrate the potential role played by muscle in SMA disease. The use of this model will allow for the understanding of the most susceptible pathogenic molecular changes in motor neurons and muscles, investigation of the effects of SMN depletion in aging, sex differences and most importantly will provide guidance for the currently aging SMA patients treated with the recently approved genetic therapies.
Funding: : This work was supported by Cure SMA/Families of SMA Canada (grant numbers KOT-1819 and KOT-2021); Muscular Dystrophy Association (USA) (grant number 575466); and Canadian Institutes of Health Research (CIHR) (grant number PJT-156379).

1. Introduction

Spinal muscular atrophy (SMA) is an autosomal inherited neurological disorder largely affecting alpha motor neurons, leading to paralysis and skeletal muscle atrophy. The genetic basis of SMA involves a deletion or mutation of the *survival motor neuron 1* (*SMN1*) gene [1], which leads to drastically reduced levels of SMN protein. The low level of SMN protein in SMA patients comes from a nearly identical copy of the *SMN1* gene, called *SMN2*. Indeed, copy number of *SMN2* is the most prominent genetic modifier of SMA severity, making clinical presentation and severity widely varied. At one end of the spectrum, type I SMA patients account for more than 50% of the incidence of SMA [2]. These patients generally have only 2 copies of *SMN2* and do not reach major motor milestones such as sitting, standing and walking [3,4]. At the other end of the spectrum, type IV SMA patients account for a very small percentage of the SMA

* Corresponding author at: Regenerative Medicine Program, Ottawa Hospital Research Institute, 501 Smyth Road, Ottawa, Ontario K1H 8L6, Canada.
E-mail address: rkothary@ohri.ca (R. Kothary).

https://doi.org/10.1016/j.ebiom.2020.102750

Research in context

Evidence before this study

Reproducing the heterogeneity of spinal muscular atrophy (SMA) in mouse models has proven difficult. In pre-clinical models, SMN depletion causes an SMA phenotype in a very narrow range of SMN level, leading to an all-or-nothing phenomenon. As such, the mice are either very sick and severe, or almost unaffected. Current mouse models of mild SMA show limited or discordant features of SMA and do not permit aging studies. This has limited our understanding of pathophysiological events in milder states of the disease and the effect of SMN depletion during aging.

Added value of this study

This study establishes a new preclinical model of mild SMA. The levels of SMN introduced from one *SMN2* allele on the $Smn^{2B/-}$ background is sufficient for recovery of normal lifespan but still allowing reduced weight, development of motor weakness, neurotransmission defects, muscle denervation and atrophy. This model also reveals new insights into sex differences, with a stronger male susceptibility. Of further interest, it also provides evidence for muscle being a contributor to disease in SMA.

Implications of all the available evidence

This model will allow for the understanding of the most susceptible pathogenic molecular changes in motor neurons and muscles, for investigation of the effects of SMN depletion in aging, for studying sex differences, and most importantly will provide guidance for the currently aging SMA patient population treated with antisense oligonucleotides or gene therapy.

population. Most of these patients harbor four or more copies of *SMN2* and start to show symptoms at 21 years of age or older [4]. Type IV SMA patients have minor functional deficits and generally a normal life expectancy [4]. For this reason, the screening and identification of these patients, as well as epidemiological data from this group has been limited [2].

In the last few years, we have witnessed the emergence of the first therapy for SMA, Spinraza, which improves symptoms and motor function in patients but cannot be considered a cure [5,6]. More recently, Zolgensma, the AAV9-SMN based gene therapy, also received FDA approval and is becoming available in the clinic [7]. It is expected that these therapeutics will increase lifespan and subsequently shift the severe infantile SMA population to a milder SMA adult population. It is unknown whether such lifespan extension will reveal new, previously unknown, comorbidities that could arise with age in this new population.

Reproducing the heterogeneity of SMA in mouse models has proven difficult [8]. The copy number of human *SMN2* in a mouse model does not result in similar severity as in human patients [8]. For example, four copies of the *SMN2* gene leads to important motor deficits in humans (some type III SMA patients) while very few defects are observed in the equivalent mouse model [8]. Interestingly, it appears that the threshold at which SMN depletion causes a SMA phenotype in mice is very narrow, with an almost all-or-nothing phenomenon, where mice are either very sick, or almost unaffected [8]. The most widely used pre-clinical models for SMA, such as the $Smn^{-/-}$;*SMN2*, the $Smn^{-/-}$;*SMN2*;$SMN^{\Delta7/\Delta7}$ and the *Taiwanese* mice (with two copies of *SMN2*) are very short-lived, with a lifespan of less than 14 days [9–11]. These mice are considered as good models of type I SMA. The $Smn^{2B/-}$ is the mildest mouse model commonly used. It contains a 3 base pair substitution in the exonic splice enhancer region of mouse *Smn* exon 7, which results in preferential splicing of this exon [12–14]. The $Smn^{2B/-}$ mouse has an average lifespan of 25 days, however it is still considered to represent severe SMA [12,15]. Even though milder models have been generated [8,16–22], their use has been limited, since many showed only a few of the hallmark SMA features (Table 1). There have also been pharmacological SMA mouse models established using low dose of SMN inducing or depleting agents (Table 2). However, these do not represent the normal physiological SMN expression through embryogenesis or adulthood as would be the case of untreated patients. Therefore, the less severe end of the clinical spectrum in SMA (type II to IV) has never been extensively studied in preclinical models. At the moment, results obtained from severe models are the only information we have, with little knowledge about molecular and pathological events in milder forms of SMA. There is a clear need for a mouse model to study milder forms of SMA, which will allow for better characterization of molecular changes within motor neurons, and to determine whether these differ in any way to those identified in severe SMA pathogenesis.

Here, we have generated $Smn^{2B/-}$;$SMN2^{+/-}$ mice, a new model for mild SMA. This mouse harbors one copy of the human *SMN2* gene on the $Smn^{2B/-}$ background and presents with nearly normal lifespan but with subtle SMA features appearing in adulthood. The $Smn^{2B/-}$;$SMN2^{+/-}$ mice are mildly weaker on motor tests and have a reduced weight starting at around 9 months of age, show evidence of electrophysiological neuronal/NMJ transmission defects marked by sex differences, structural NMJ aberrations in the diaphragm and muscle contraction/relaxation defects. Overall, this is the first mouse model that reproduces most of the SMA classical features, while offering additional insight into sex differences. This model will also offer valuable information concerning SMN depletion in aging.

2. Materials and methods

2.1. Study design

Upon generation of the mouse model, three pre-specified objectives were: (1) identify whether $Smn^{2B/-}$;$SMN2^{+/-}$ mice display motor weakness, (2) assess for hallmark neuronal and muscular features of SMA in the mouse model, (3) assess extra-neuronal involvement in the mild model. All objectives were pursued in a simultaneous manner. Sex differences were identified as a late finding and were not initially pursued as a study objective. Behavioral data in the adult phase, echoMRI and lipid quantification were outsourced, and, thus, analyzes were performed in a blinded fashion. Quantification of spinal cord and muscle histology (apart from the qualitative analysis) were also performed in a blinded fashion. Sample size calculations were not performed. *N* number is described in each figure legend. Statistical approach is as described below and in figure captions.

2.2. Mouse model generation and husbandry

$Smn^{2B/-}$;$SMN2^{+/-}$ and $Smn^{2B/+}$;$SMN2^{+/-}$ mice were generated by crossing a $Smn^{2B/2B}$ mouse (FVB background) [15] with a $Smn^{+/-}$;*SMN2* mouse (FVB background - Jackson Laboratory [11]). Note that the human *SMN2* transgene in the latter mouse is the *(SMN2)89Ahmb* allele that was mapped to mouse chromosome 6 [23]. $Smn^{+/-}$;$SMN2^{+/+}$ mice were crossed to $Smn^{2B/2B}$;$SMN2^{-/-}$ mice to obtain $Smn^{2B/-}$;$SMN2^{+/-}$ animals. The following primers were used for genotyping: Common forward primer (5′ GGG TTG ATC TAG GGA CTT TGA G 3′), reverse wild type primer (5′ GGG AGT TGT GGC ATT CTT CT 3′), and reverse SMA primer (5′ GCT GAT TTG TGT AGT CGG TTT ATG 3′). Young wild type (WT) mice were 12–16 weeks old B6.SJL-*Ptprca Pepcb*/BoyJ mice that harbor the differential *Ptprca* pan leukocyte marker commonly known

Table 1
Review of mouse models of mild SMA.

Mouse model	Follow-up time	Lifespan	Neuronal pathology	NMJ pathology	Muscle size	Motor function	Extra-neuronal findings	Tail length	Ref.
SMN^{RT}	100 d	34 d	↓ proprioceptive synapses #MN: same	↑ immaturity ↓ innervation	↓	↓	IVS ↓ ↑ heart fibrosis	N/A	[17]
Burgheron	6 m	~3 m	↓ In CMAP/SMUP no axonal loss #MN: N/A	↓ size ↑ immaturity	=	N/A	Heart defects	Full loss	[16]
Taiwanese (4 copies)	15 m	~12 m	↓ CMAP #MN: ↓	N/A	↓	↓	N/A	Shorter tails	[21]
$Smn1^{C/C}$	60 w	>12 m	↓ synaptic efficacy no axonal loss #MN: N/A	Slightly abnormal	N/A	Normal	↓ HR ↓ BMD	necrosis	[20]
SmnC>T/C>T	800 d	Normal	Similar #MN: same	No abnormalities identified	↑	↓	N/A	N/A	[18]
A2G $Smn^{-/-}$;SMN2	N/A	227 d	↓ CMAP amplitude #MN: ↓	↑ sprouting	↓	N/A	N/A	N/A	[19]
A111G $Smn^{-/-}$;SMN2	1.5 y	Normal	No axonal loss #MN: N/A	N/A	↑	N/A	N/A	N/A	[22]
$Smn^{+/-}$	1 y	N/A	Degenerating axons CMAP normal #MN: ↓	↑ sprouting Mild denervation	N/A	Normal	N/A	N/A	[47,48]

Abbreviations : d – days, m – months, y – years, N/A – not available, CMAP – compound motor action potential, SMUP – single motor unit potentials, MN – motor neurons, NMJ – neuromuscular junction, IVS – interventricular septum, HR – heart rate, BMD – bone mineral density.

Table 2
Review of pharmalogically-induced mouse models of mild SMA.

Mouse model	Follow-up time	Lifespan	Neuronal pathology	NMJ pathology	Muscle size	Motor function	Extra-neuronal findings	Tail length	Ref.
Taiwanese + PMO25 (10 ug/g)	~125 d	22 d	#MN: no change	↓ innervation ↓ size	↓	↓	N/A	N/A	[71]
Taiwanese + PMO25 (10 ug/g) q2wks	~150 d	~92 d	#MN: no change	↓ size	↓	=	N/A	None	[71]
SmnΔ7 + 0.1 mg/kg SMN-C3*	~35 d	~28 d	Axonal loss #MN: N/A	↓ innervation	↓	↓	N/A	Shorter tails	[72,73]
SmnΔ7 + 3 mg/kg SMN-C3	N/A	Near normal	No axonal loss #MN: N/A	↓ innervation	↓ in some muscles	↓	N/A	Shorter tails	[72,73]
Taiwanese (4 copies) + ASO-20-37 (ICV)	~500 d	~90-130 d	#MN: ↓ or normal MN size: ↓	Varicosities, endplate fragmentation No denervation	Normal	↓	No heart or liver abnormalities	N/A	[49]
Taiwanese (4 copies) + ASO-20-37 (IP)	~110 d	~90 d	#MN: ↓	N/A	N/A	No change	*Heart*: LV size reduction, IVS hypertrophy *Liver*: Necrosis, degeneration, regeneration	N/A	[49]

Abbreviations : d – days, N/A – not available, MN – motor neurons, NMJ – neuromuscular junction, IVS – interventricular septum, PMO -, q2wks – every two weeks, ICV – intracerebroventricular, IP – intraperitoneal, LV – left ventricle, * interchangeable with SMN-C1 (a closely related molecule).

as CD45.1, useful for discrimination of host versus donor in transplantation experiments. These mice are otherwise WT. All mice were housed at the University of Ottawa Animal Facility and cared for according to the Canadian Council on Animal Care. Experimentation and breeding were performed under protocol OHRI-1948 and OHRI-1927.

2.3. In vivo *measurement and behavioral testing*

Tail length was taken with a ruler by stretching the tail to its full length. The same group of mice was subjected to an array of behavioral tests throughout development (as described below). All behavioral testing was performed by one single examiner per time point with the assistance of a second examiner for time recording for the tests involving young mice. Each mouse was tattooed between P3-P5 to allow longitudinal examination of motor function. Tests were administered in the following order: (1) righting reflex, (2) pen test, and (3) inverted mesh/wire grip. All tests were performed on the same day and testing occurred every two days. The righting reflex was performed from P12 to P18, the pen test from P18 to P24 and inverted mesh grip from P12 to P30. Each test was repeated 3 times to ensure reliable measures. Groups of 3 mice were taken at a time, allowing for a period of rest before having the test repeated. Righting reflex followed a similar protocol as previously described in Treat-NMD neuromuscular network (SOP MD_M.2.2.002). The pen test followed a similar protocol as previously described in Treat-NMD neuromuscular network (SOP SMA_M.2.1.001). A maximum of 30 s on the pen was defined as a perfect score. The inverted mesh/wire followed a slightly modified protocol than previously described in Treat-NMD neuromuscular network (SOP SMA_M.2.1.002). Briefly, a mesh grip (hole of 1 mm^2) is used from P13 to P19. At P21, the mesh grip was changed to a wire cage top to provide more space for the growing mice to hold on to. Termination of this test was set at 60 s. The rotarod and grip strength were performed by the behavioral core of the University of Ottawa every two months. One test per day was performed and the assays were separated by at least one day of rest. Forepaw grip strength was measured using a Chatillon grip meter (Columbus Instruments, Columbus, OH, USA). Rotarod performance

(IITC Life Sciences, Woodland Hills, CA, USA) was done on two consecutive days, with each day consisting of 4 trials of 1−45 rpm accelerating over 60 s with an inter-trial interval of 10 min. The same cohort of mice was assessed by EchoMRI for body composition (EchoMRI LLC, Houston, TX, USA). Mice that develop circling over their lifetime were removed from analysis of weight, grip strength, rotarod, and echoMRI after the onset of circling. All testing by the behavioral core was performed in a blinded fashion.

2.4. Gross morphology of organs

The mouse measurements for normalization were done prior to dissection using a ruler for the length of the mouse and a scale for its weight. Organs were weighed with a scale. Tissues were then fixed in 10% formalin for 24−48 h and transferred to 70% ethanol for long-term storage.

2.5. Immunoblotting

Total protein lysate was collected by homogenization of flash frozen spinal cord, liver and hindlimb muscles in RIPA lysis buffer (Cell Signaling). Protein concentrations were determined using the Bradford assay (Bio-Rad). Protein extracts were subjected to sodium dodecyl sulfate polyacrylamide gel electrophoresis and examined by immunoblot, as previously described [24] with modified blocking conditions where Odyssey blocking buffer (Li-Cor 927−40000) replaced 5% milk. Revert Total protein stain (Li-Cor 926−11010) was used as per the manufacturer's protocol. Primary antibodies used were as follows: Anti-Smn (BD Transduction, 610647 - 1:1000−2000), alpha-tubulin (Abcam, ab4074 - 1:5000−15,000) and ubiquitin (Biolegend P4D1-1:1500), Secondary antibodies used were IRDye (Li-Cor) 680 or 800 (Li-Cor - 1:10,000 to 1:20,000). Signals were detected with Odyssey CLx (Li-Cor). Results were normalized to total protein or tubulin. Full western blots can be visualized in Supp. Fig. 6.

2.6. Tissue processing and staining

Spleens, tibialis anterior (TA) muscle and livers were fixed in formalin (1:10 dilution buffered, from Protocol, cat #245-684) for 48 h while spinal cords were fixed for 96 h at 4 °C and then transferred in 70% ethanol at 4 °C until processing. All samples were processed at the University of Ottawa (Department of Pathology and Laboratory Medicine) and embedded in wax using a LOGOS microwave hybrid tissue processor. Paraffin block tissues were cut with a microtome at 3−4 μm of thickness and stained for H&E using a Leica autostainer XL Leica CV5030. Spinal cord sections were stained with cresyl violet. Stained samples were scanned with a MIRAX MIDI digital slide scanner (Zeiss). Images were acquired using 3DHISTECH Panoramic Viewer 1.15.4 at different magnifications.

For choline acetyltransferase (ChAT) staining of motor neurons, 18-month-old male $Smn^{2B/-}$;$SMN2^{+/-}$ and $Smn^{2B/+}$;$SMN2^{+/-}$ mice (three of each genotype) were euthanized and lower lumbar spinal cords were dissected and fixed in 4% paraformaldehyde (PFA) in PBS overnight. The samples were incubated in 30% sucrose in PBS for 24 h, embedded in OCT, and then frozen. For each spinal cord sample, ten cryosections of 16 μm thickness with an interval of 128 μm were mounted on slides and kept at −20 °C until staining. The slides were air dried at room temperature (RT) for 24 h and rinsed with TBST for 5 min. Samples were permeabilized in 0.3% Triton X-100 in PBS for 30 min, then blocked in 1x Power Block (BioGenex, Fremont, CA) for 20 min at RT. Samples were incubated with a goat anti-ChAT antibody at a dilution of 1:100 (EMD, Millipore, #AB144P) in 1% BSA and 0.3% Triton X-100 in PBS for 3 nights at 4 °C. After the first antibody incubation, slides were washed twice for 10 min with TBST at RT. Samples were then incubated with Alexa Fluor 555 donkey anti-goat IgG (1:200, Life Technologies, Carlsbad, California) for 2 h at RT in 10% donkey serum and 0.3% TritonX-100 in PBS in a humid chamber. Nuclei were counterstained with 4′,6-diamidino-2-phenylindole (DAPI) 1:1000 in TBST for 5 min. Finally, slides were carefully rinsed twice for 10 min with TBST and slides were mounted with Fluorescent Mounting Medium (Dako) and examined under fluorescence using a Zeiss microscope equipped with an AxioCam HRm camera. For our quantification, a total of 20 ventral horns (10 slides) were quantified and only ChAT-positive motor neurons (diameter ≥ 20 μm) were counted.

2.7. Descriptive histopathological analysis and quantification of the spinal cord and skeletal muscle

Quantification of motor neuron number and size was performed on a total of 5 sections separated by 8 sections each per animal. The spinal cord sections assessed were from the lumbar region. The *N* number represents the number of animals and not the number of sections counted. Three criteria were used for motor neuron identification and ensuring appropriate counts: location in the ventral horn, presence of nucleolus, and cells were at least 200 or 350 μm^2 in cross-sectional area for the two distinct analyzes performed. For the quantification of the TA muscle about 100−150 fibers were counted in different areas of the muscle section to ensure appropriate coverage. A minimum of 200−600 fibers total were counted at 6 and 12 months. At 18 months, the size of the muscle for some SMA mice would only allow for one image and thus only 100 fibers were counted. Frozen sample slides from the TA muscle were stained with the following: hematoxylin and eosin, and reduced nicotinamide adenine dinucleotide-tetrazolium reductase (NADH). The available samples were from male and female $Smn^{2B/+}$;$SMN2^{+/-}$ and $Smn^{2B/-}$;$SMN2^{+/-}$ mice at 6, 12, and 18 months of age. On the paraffin-embedded samples of the TA skeletal muscle, the number of atrophic fibers at 6, 12 and 18 months of age was assessed in 20 high power fields (400x) or, if the sample was too small, on 10 fields doubling the number. Twenty $Smn^{2B/+}$;$SMN2^{+/-}$ cases, 11 females and 9 males, and 22 $Smn^{2B/-}$;$SMN2^{+/-}$ cases, 8 females and 14 males were used in the analysis.

2.8. Sciatic nerve preparation

Sciatic nerves were collected from $Smn^{2B/-}$;$SMN2^{+/-}$ and $Smn^{2B/+}$;$SMN2^{+/-}$ mice at 18 months and fixed in Karnovsky's fixative (4% PFA, 2% glutaraldehyde, and 0.1 M cacodylate buffer in PBS, pH 7.4) for a minimum of 4 h at 4 °C. After fixation, sciatic nerves were cut under a stereomicroscope into straight segments of 1 mm of length. Segments were subsequently washed 2 times in 0.1 M cacodylate buffer for 1 h and once overnight at RT. After 1 h of post-fixation in 1% osmium tetroxide in 0.1 M cacodylate buffer at 4 °C, specimens were washed twice for 5 min each in distilled water. Samples were dehydrated, infiltrated in spurr monomer (Electron Microscopy Sciences) with 3 changes over 24 h at RT and embedded in liquid spurr resin at 70 °C overnight. Sciatic nerve sections of 0.3 μm were mounted on glass slides and stained with toluidine blue, and then examined by light microscopy. Total number of axons by sciatic nerve cross-section was quantified using ImageJ software.

2.9. Neuromuscular junction analysis

Male $Smn^{2B/-}$;$SMN2^{+/-}$ and $Smn^{2B/+}$;$SMN2^{+/-}$ mice at 18 months were anesthetized by CO_2 and then rapidly sacrificed. The whole diaphragm was dissected intact still attached at the front to the xiphoid process and laterally along the ribs and in the back to back muscles and vertebra. The sample was rinsed with distilled water and transferred to a petri dish containing PBS. Each diaphragm was divided in 3 regions (left lateral, ventral top and right lateral). We placed the preparation in a well of a 12-well plate with PBS on ice. Samples were fixed for 10 min with 2% PFA and rinsed with PBS. Samples

were permeabilized with 0.5% Triton X-100 in PBS for 3 h at RT. Motor end-plates were stained with alpha-bungarotoxin tetramethylrhodamine conjugate (Invitrogen T1175) (dil:1:1000−2000) for 30 min at RT in the dark. Diaphragm segments were washed 3 × 15 min in PBS and kept overnight in PBS (12-well plates with aluminum foil) on a VWR advanced digital shaker at low speed. Diaphragms were then permeabilized with 1% Triton X-100 in PBS for 30 min at RT. Following that samples were blocked with 10% goat serum, 1% BSA and 0.1% Triton X-100 in PBS. Diaphragm segments were incubated for a period of 90 min with neurofilament antibody (purified anti-neurofilament marker (Pan-axonal cocktail), Biolegend, SMI 312, 1:200) and mouse anti-SV2 (Developmental Studies Hybridoma Banks, 1:200) in 1% BSA, 0.1% Triton X-100 in PBS. Samples were washed 3 × 10 min with the first wash solution (0.1% Triton X-100 and 0.1% BSA in PBS). Samples were incubated with the secondary antibody Alexa Fluor 488 goat anti-mouse 1:200 in 10% goat serum and 0.1% Triton X-100 in PBS for 1 h at RT (with aluminum foil). Diaphragm segments were washed 3 × 10 min with a second wash solution (0.1% Triton X-100 in PBS). Finally, samples were rinsed in water and slides were mounted with Fluorescent Mounting Medium (Dako). NMJs were examined under fluorescence at different magnifications (with z-stack) using a Zeiss Axioplan microscope equipped with an AxioCam HRm camera. For our analysis, a minimum of 1000 NMJs were examined by diaphragm from each mouse, ensuring careful examination of various regions of the diaphragm for each sample.

2.10. Lipid quantification

Tissue lipid analysis for quantification and profiles were performed at the Vanderbilt Mouse Metabolic Phenotyping Center in a blinded fashion. Lipids were extracted and analyzed as described [25−27].

2.11. Electrophysiology

A nerve-soleus muscle preparation was used for this study as previously reported [28]. Briefly, mice were anesthetized with a single intraperitoneal injection of 2.2 mg ketamine/0.4 mg xylazine/0.22 mg acepromazine per 10 g of animal body weight and sacrificed by cervical dislocation. The soleus and its associated nerve were then dissected in continuously oxygenated physiological control solution (118.5 mM NaCl, 4.7 mM KCl, 1.3 mM $CaCl_2$, 3.1 mM $MgCl_2$, 25 mM $NaHCO_3$, 2 mM NaH_2PO_4, 5.5 mM D-glucose and continuously bubbled with 95% O_2:5% CO_2 to maintain pH at 7.4). The nerve-muscle preparation was then transferred and positioned into a 2 ml plexiglass chamber where it was fixed to the stationary hook and a force transducer (model 402A; Aurora Scientific Canada). Experimental temperature was kept at 37 °C and physiological control solution (described above) continuously ran through the chamber at 15 ml/min. Data were digitized at a sampling rate of 5 kHz using a KCP13104 data acquisition system (Keithley Instruments Inc, U.S.A.). Muscle length giving maximal force was identified and muscle was allowed to stabilize for 30 min. Following this, the nerve was stimulated via a suction electrode containing platinum wires connected to a Grass S88 stimulator and Grass SIU5 isolation unit (Grass Technologies, U.S.A). Twitch contractions were elicited with a single stimulation or tetanic contractions were elicited with a 400 ms train of 0.3 ms, 1 V (supramaximal voltage) pulses at 1 to 180 Hz. Stimulations were performed every 5 min. Maximal force (180 Hz stimulation) was first measured followed by a force-frequency curve. Muscles were then exposed to 30 μM tubocurarine hydrochloride pentahydrate (Sigma 93,750, Oakville, ON, Canada) to completely block neural transmission at the neuromuscular junction. This was confirmed when no force was generated by the muscle when the nerve was stimulated. Muscles were then directly stimulated by two platinum wire located on the opposite side of the muscle also connected to a Grass S88 stimulator and Grass SIU5 isolation unit (Grass Technologies, U.S.A.). Twitch and tetanic contractions were again elicited, except that the stimulation voltage was increased. The following parameters were later analyzed as follows: Twitch and tetanic force was calculated as the difference between the resting baseline force and force generated upon stimulation and normalized to N/cm^2 using muscles length and weight; half-rise time was calculated as the time interval from the first stimulation to the time force had reached 50% of the contraction amplitude; twitch half-relaxation time was calculated as the time interval between the time force reached a peak and force had decayed by 50% while for a tetanic contraction half-relaxation time was calculated as the time interval between the last stimulation and the time force had decayed by 50%; width represented the time interval between half-rise and half-relaxation time; maximum rate of force development and relaxation was obtained by first applying a linear regression analysis to every 10 data points to calculate the rate of force change over time and then finding the maximum and minimum peak during the contracting and relaxation phase, respectively.

2.12. Ultrasonography

Mice were shaved and Veet was used to ensure complete hair removal, allowing for adequate ultrasonographic quality. Mice were then anesthetized using continuous 3% isoflurane inhalation and placed on warming movable station where each limb was taped to the station to allow heart rate monitoring. A rectal probe was inserted for temperature monitoring and temperature was maintained between 36 °C and 38.5 °C. Ultrasonography was performed using a MS400 or MS550 transducer and the VEVO 2100 (FujiFilm VisualSonics, Toronto, Canada). M-mode acquisition was obtained ensuring the visualization of the papillary muscles for consistency of depth the slice. Quantification was performed by left ventricular trace to provide heart rate, stroke volume, cardiac output, ejection fraction and fractional shortening. For the splenic artery measurement, the position of the mice remained the same or repositioned in a right lateral decubitus in difficult identification of splenic anatomy and vascularity. As such, heart rate and temperature were not actively monitored during this part of the experiment. The spleen was identified under B-mode imaging, and doppler was used to identify the splenic artery. Peak flow velocity and heart rate was sampled and quantified as recommended by FujiFilm VisualSonics consultant.

2.13. Statistical analyzes

Data are presented as the mean ± standard error of the mean. A Student's *t*-test was performed using Microsoft Excel or GraphPad Prism 7 to compare the means of data when only two groups were compared (i.e., $Smn^{2B/+};SMN2^{+/-}$ and $Smn^{2B/-};SMN2^{+/-}$ mice). Matched two-way ANOVA with Geisser-Greenhouse correction (no assumption of sphericity) was used with complete data sets (i.e., Supp Fig. 1). Matched two-way ANOVA with mixed effects model was performed where values were missing (in case of circling or death) (i.e., Fig. 1). Ordinary two-way ANOVA was used for analysis of motor neuron and skeletal muscle histology. Sidak's or Tukey's method was used for multiple comparisons depending on the characteristics of the dataset. One-way ANOVA analysis was used to distinguish differences between more than two groups when multiple comparisons were necessary (i.e., young wild type vs. $Smn^{2B/+};SMN2^{+/-}$ and $Smn^{2B/-};SMN2^{+/-}$ mice). The post-test used for the ANOVA was Tukey. Significance was set at $P \leq 0.05$ for *, $P \leq 0.01$ for **, $P \leq 0.001$ for *** and $P \leq 0.0001$ for ****.

2.14. Data availability

All data will be made available upon contacting the corresponding author.

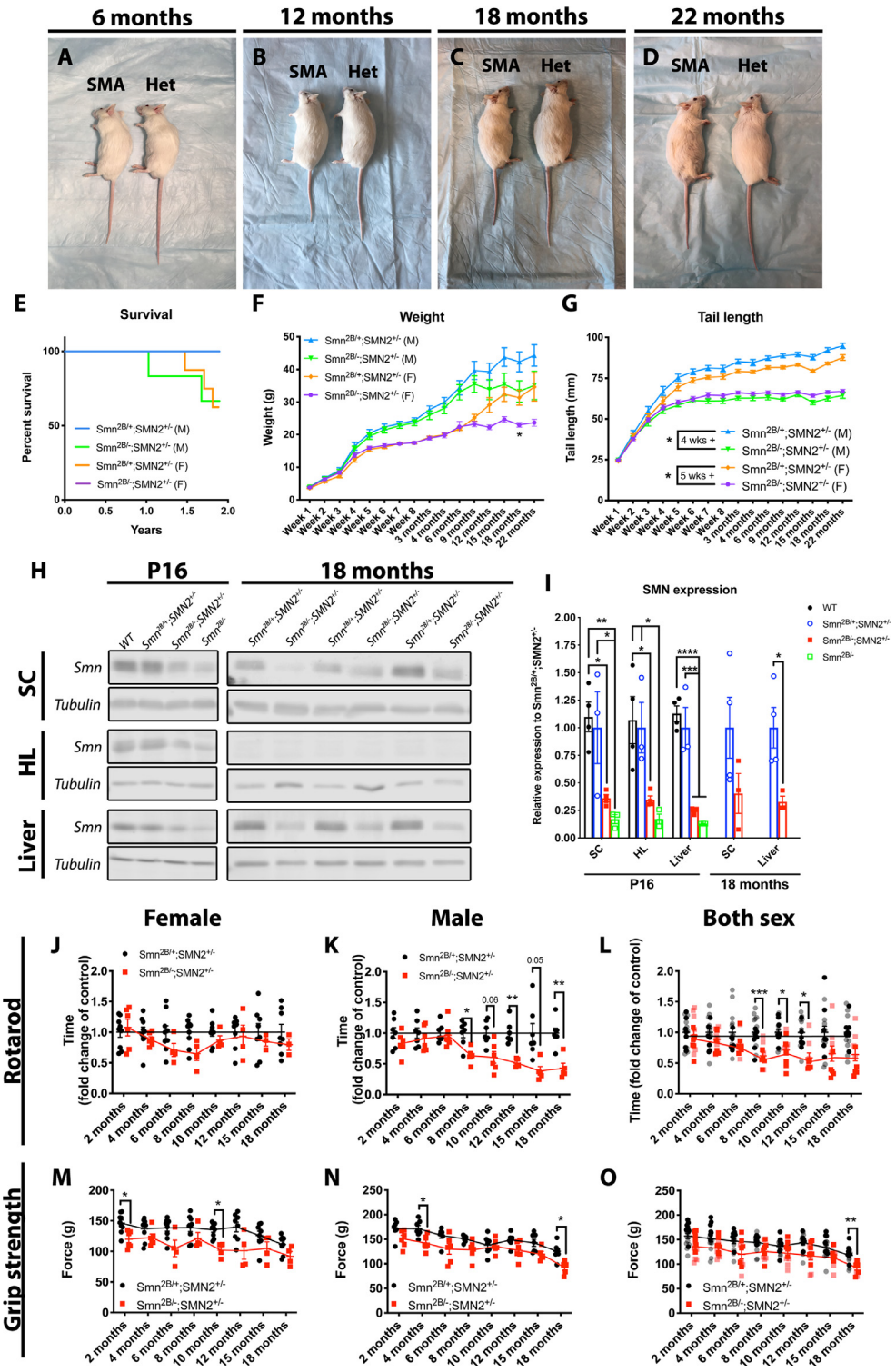

Fig. 1. *Smn*$^{2B/-}$;*SMN2*$^{+/-}$ mice live a normal life but have shorter tails, reduced weight gain, and display sex-specific motor impairment. (A-D) Representative images of *Smn*$^{2B/-}$;*SMN2*$^{+/-}$ (SMA) and *Smn*$^{2B/+}$;*SMN2*$^{+/-}$ (Het) mice aged between 6 months and 22 months. (E) Survival was largely unchanged between *Smn*$^{2B/-}$;*SMN2*$^{+/-}$ and *Smn*$^{2B/+}$;*SMN2*$^{+/-}$ mice, although some mutant male mice died late in life before any of the others in the cohort. (F) Reduced weight gain was obvious by 12 and 15 months for female and male *Smn*$^{2B/-}$;*SMN2*$^{+/-}$ mice. (G) *Smn*$^{2B/-}$;*SMN2*$^{+/-}$ mice showed reduced tail length at 4 weeks of age and this persisted for the remainder of their lives. (H-I) SMN protein levels in the *Smn*$^{2B/-}$;*SMN2*$^{+/-}$ mice were about 35% of the *Smn*$^{2B/+}$;*SMN2*$^{+/-}$ mice in all tissues analyzed. (J-L) When both sexes were analyzed together, impairment on rotarod test was identified by 8 months of age and was sustained in *Smn*$^{2B/-}$;*SMN2*$^{+/-}$ mice. When the data is stratified based on sex, these impairments were more readily seen in the male population in comparison to the female *Smn*$^{2B/-}$;*SMN2*$^{+/-}$ mice. (M-O) Modest reduction of grip strength was nearly constantly seen over time in *Smn*$^{2B/-}$;*SMN2*$^{+/-}$ mice in both males and females. (The *n* value for each study is as follows: (E-G, J-O) *Smn*$^{2B/+}$;*SMN2*$^{+/-}$ female mice (6–9), *Smn*$^{2B/-}$;*SMN2*$^{+/-}$ female mice (4–6), *Smn*$^{2B/+}$;*SMN2*$^{+/-}$ male mice (7), *Smn*$^{2B/-}$;*SMN2*$^{+/-}$ male mice (4–6); (H-I) 3–4. Average ± SEM displayed, statistical analysis (E) Mantel-Cox test, (F-G, J-O) two-way ANOVA with mixed effects model with Geisser-Greenhouse correction and Sidak's multiple comparisons test (I) One-way ANOVA with Tukey multiple comparison tests for P16 and unpaired *t*-test for 18 months, $P \leq 0.05$ for *, $P \leq 0.01$ for ** and $P \leq 0.001$ for ***).

3. Results

3.1. The Smn$^{2B/-}$;SMN2$^{+/-}$ *mice have a normal life span, reduced tail length and progressive muscle weakness with age*

Mouse models of mild SMA have been extremely challenging to generate [8,16–22]. We have recently produced congenic *Smn$^{2B/2B}$* mice on both the FVB and C57BL6 genetic backgrounds [15]. This allowed pairing of the *Smn$^{2B/2B}$* (FVB) with the *Smn$^{+/-}$;SMN2* (FVB), giving a progeny of *Smn$^{2B/+}$;SMN2$^{+/-}$* and *Smn$^{2B/-}$;SMN2$^{+/-}$* mice on a congenic FVB background. We initially characterized *Smn$^{2B/-}$;SMN2$^{+/-}$* mice for survival, SMN levels, weight and motor behavior. *Smn$^{2B/-}$;SMN2$^{+/-}$* mice had a lifespan and morphology quite similar to the control *Smn$^{2B/+}$;SMN2$^{+/-}$* mice (Fig. 1A-E). Nevertheless, some male *Smn$^{2B/-}$;SMN2$^{+/-}$* mice succumbed earlier than female mice during the length of the study (Fig. 1E). We observed a slowing down of weight gain in *Smn$^{2B/-}$;SMN2$^{+/-}$* mice beginning at 6 months of age, however it did not reach significance apart from one time point in females (18 months) (Fig. 1F). We also noticed a considerable reduction of tail length, a feature present in many other mouse models of SMA [16,17,21,29]. Reduced tail length was observed as soon as 4 weeks of age and was constant over time, regardless of sex (Fig. 1G). We have previously shown that *Smn$^{2B/-}$;SMN2$^{+/-}$* mice (FVB) display about 10% more SMN protein than that in *Smn$^{2B/-}$* mice (C57BL6) (25% vs. 15% of SMN protein compared to wild type) [30]. We have now analyzed SMN levels at P16 between WT, *Smn$^{2B/+}$;SMN2$^{+/-}$*, *Smn$^{2B/-}$;SMN2$^{+/-}$* and *Smn$^{2B/-}$* and at 18 months between the *Smn$^{2B/+}$;SMN2$^{+/-}$* and *Smn$^{2B/-}$;SMN2$^{+/-}$* mice across various tissues (Fig. 1H-I). WT animals had only slightly higher levels than *Smn$^{2B/+}$;SMN2$^{+/-}$* across all tissues assessed (Fig. 1H-I). At P16, SMN levels in the *Smn$^{2B/-}$;SMN2$^{+/-}$* mice was at approximately 35% for the spinal cord and hindlimb muscle and only 26% for the liver in comparison to the *Smn$^{2B/+}$;SMN2$^{+/-}$* tissues (Fig. 1H–I). The SMN protein level in these

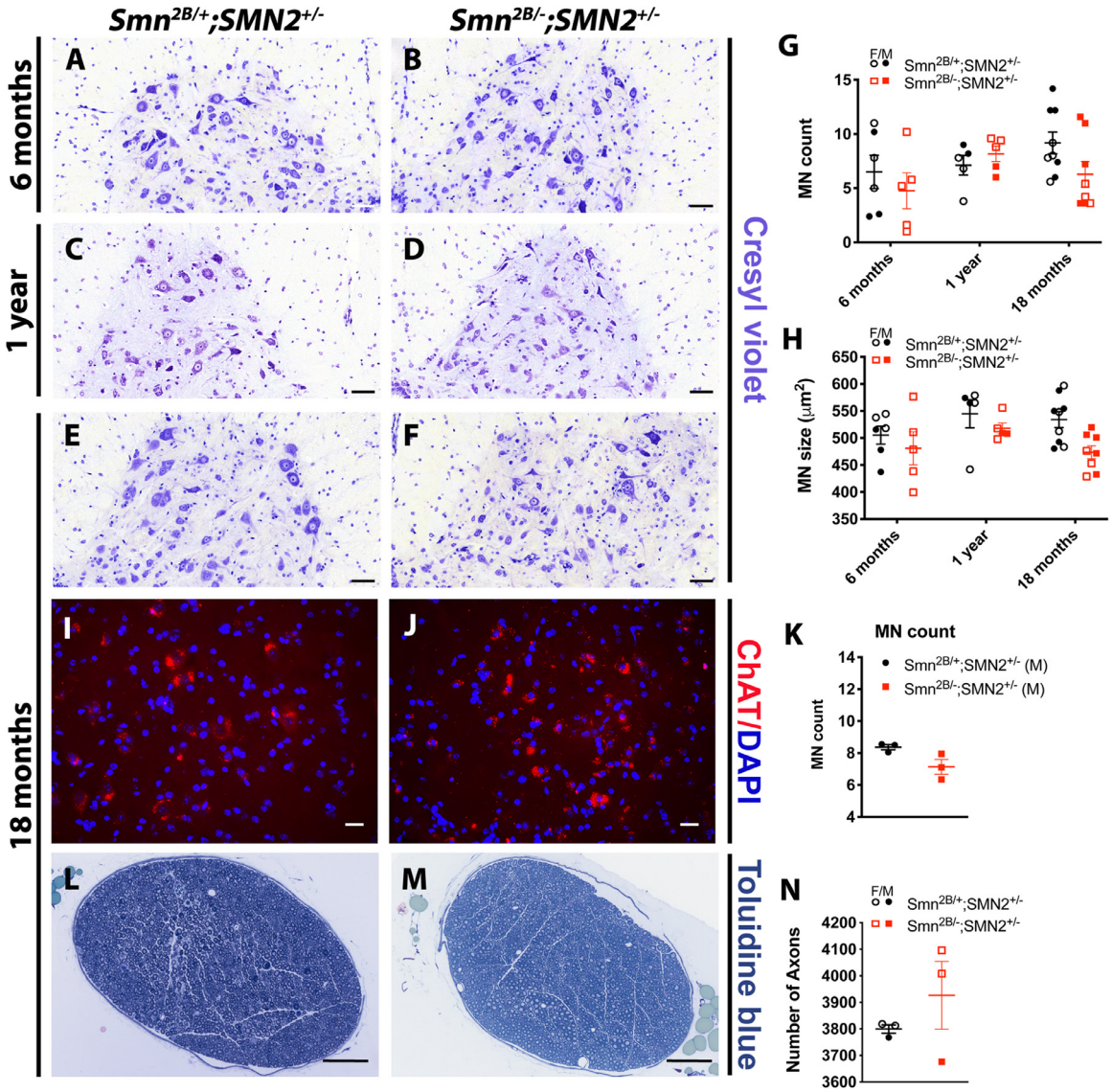

Fig. 2. *Smn$^{2B/-}$;SMN2$^{+/-}$* mice do not display any detectable motor neuron loss. Representative 30X images (A-F) and quantification (G-H) of the motor neuron number and size in spinal cord sections from *Smn$^{2B/+}$;SMN2$^{+/-}$* and *Smn$^{2B/-}$;SMN2$^{+/-}$* mice at 6, 12 and 18 months. (I-K) ChAT staining of 18 month male *Smn$^{2B/+}$;SMN2$^{+/-}$* and *Smn$^{2B/-}$;SMN2$^{+/-}$* lumbar spinal cord sections showed no difference in motor neuron count. (L-N) Axonal loss was not observed in the sciatic nerves of *Smn$^{2B/-}$;SMN2$^{+/-}$* mice. Scale bars represent 50 μm (A-F) 20 μm (I-J) and 100 μm (L-M) (The *n* value for A-H was 5–9 and represents biological replicates (i.e., number of mice). Note that 5 sections of spinal cord from each animal were analyzed. (I-N) *N* = 3 (only males in I-K). Average ± SEM displayed. Note that for (I-K) 10 sections of spinal cord from each animal were analyzed. Data in (A-H) analyzed with ordinary two-way ANOVA with Tukey post-test for multiple comparison and sex difference at 18 months assessed by one-way ANOVA with Tukey post-test for multiple comparison, and (I-N) unpaired student *t*-test.

tissues ranged between 13 and 17% in the *Smn*$^{2B/-}$ mice at P16. At 18 months, we were unable to detect SMN in the hindlimb using western blot analysis (Fig. 1H–I). However, despite some variability, SMN protein levels ranged between 33% and 40% in the *Smn*$^{2B/-}$;*SMN2*$^{+/-}$ liver and spinal cord, respectively, in comparison to *Smn*$^{2B/+}$;*SMN2*$^{+/-}$ mice (Fig. 1H-I). This closely match the results observed in P16 mice.

We next investigated whether motor functions were affected in *Smn*$^{2B/-}$;*SMN2*$^{+/-}$ mice. We did not see any difference between *Smn*$^{2B/-}$;*SMN2*$^{+/-}$ mice and control *Smn*$^{2B/+}$;*SMN2*$^{+/-}$ mice in righting reflex, pen test or mesh grip during early life (Supp Fig. 1A-C). We next moved to adult appropriate motor function tests such as grip strength and rotarod. Motor impairment was readily identified in rotarod test at 8 months of age for the male *Smn*$^{2B/-}$;*SMN2*$^{+/-}$ mice but not the female *Smn*$^{2B/-}$;*SMN2*$^{+/-}$ mice (Fig. 1J-L). Grip strength measurements revealed modest diminished force, however sustained, as early as 2 months of age in *Smn*$^{2B/-}$;*SMN2*$^{+/-}$ mice for both sexes (Fig. 1M–O). However, the decreased force did not reach statistical significance. It is important to keep in mind that the shorter tail length may act as a confounding factor in the rotarod test. However, the tails of male *Smn*$^{2B/-}$;*SMN2*$^{+/-}$ mice, albeit shorter, remained constant over time while their performance worsened on the rotarod test (Fig. 1K). In addition, female mice did not show similar difficulties in rotarod despite having a short tail (Fig. 1J) and it has been previously shown that performance is not impaired by tail cutting [21]. Therefore, we conclude that motor weakness is present during adulthood in our new mouse model, reminiscent of what is observed in type IV SMA patients. Altogether, these features are very consistent with delayed onset of SMA pathology, similar to less severe type III and IV SMA patients.

3.2. The Smn$^{2B/-}$;SMN2$^{+/-}$ mice do not show motor neuron loss but have neurogenic atrophy

Next, we investigated motor neuron number and muscle pathology, two classical hallmarks of SMA. In the lumbar region of the spinal cord, we did not detect any differences in motor neuron number or motor neuron size at all time points between *Smn*$^{2B/+}$;*SMN2*$^{+/-}$ and *Smn*$^{2B/-}$;*SMN2*$^{+/-}$ mice (Fig. 2). We did not see any sex differences at 18 months of age in the *Smn*$^{2B/-}$;*SMN2*$^{+/-}$ mice (Fig. 2G-H). Given that SMA motor neurons can be smaller than control, we used two different cut-offs for area (200 μm^2 and 350 μm^2). However, we did not observe any difference regardless of which cut-off was used (data not shown, 350 μm^2 cut-off used in Fig. 2H). To ensure the accuracy of our quantification, we stained lumbar sections from 18 month old mice for ChAT, a marker specific to motor neurons (Fig. 2I-K). This analysis gave similar results to those obtained using cresyl violet staining. Similarly, axon number in the sciatic nerve was not different between *Smn*$^{2B/+}$;*SMN2*$^{+/-}$ and *Smn*$^{2B/-}$;*SMN2*$^{+/-}$ mice at 18 months (Fig. 2L-N).

We next assessed whether any neurogenic atrophy is present in TA muscle of *Smn*$^{2B/-}$;*SMN2*$^{+/-}$ mice (Fig. 3). Analysis of a fiber size

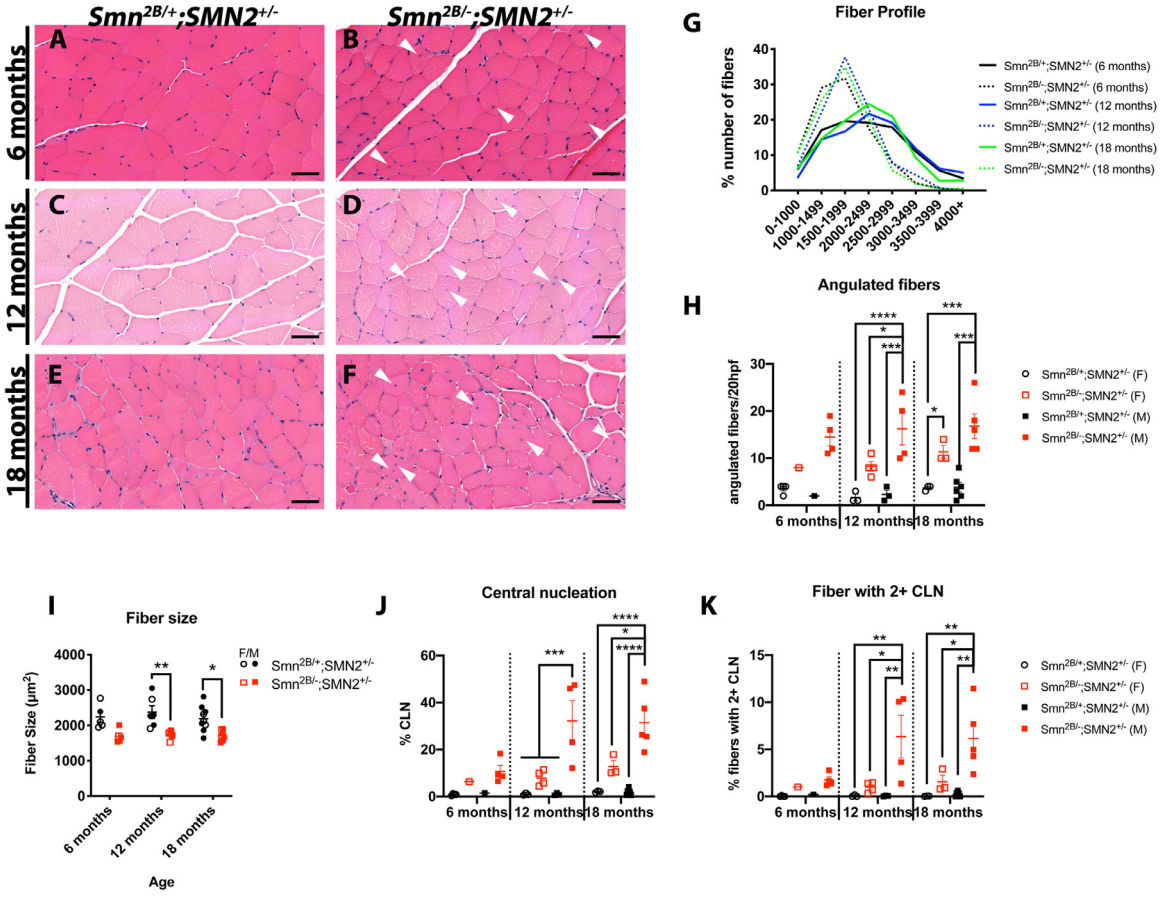

Fig. 3. *Smn*$^{2B/-}$;*SMN2*$^{+/-}$ muscle display neurogenic atrophy and prominent central nucleation. Representative images of the *tibialis anterior* (TA) muscle of *Smn*$^{2B/+}$;*SMN2*$^{+/-}$ and *Smn*$^{2B/-}$;*SMN2*$^{+/-}$ mice at 6 months (A-B), 12 months (C-D), and 18 months (E-F). The fiber size profile distribution (G) is shifted to the left in *Smn*$^{2B/-}$;*SMN2*$^{+/-}$ mice at all ages analyzed. (H) In the *Smn*$^{2B/-}$;*SMN2*$^{+/-}$ mice, the atrophic fibers were more than double in the female and more than three to four times in the males in comparison to *Smn*$^{2B/+}$;*SMN2*$^{+/-}$ mice. (I) There is a reduction in fiber size in *Smn*$^{2B/-}$;*SMN2*$^{+/-}$ mice. (J) Central nucleation was constantly and progressively increased from 6 months to 18 months. (K) Many fibers from *Smn*$^{2B/-}$;*SMN2*$^{+/-}$ mice had 2 or more centrally located nuclei, a feature worse in males. Scale bars represent 50 µm in A-F. (The *n* value is (H,J,K) 3–6, except for 6 months where *N* = 1–4 (G,I) 5–9, average ± SEM displayed, Ordinary two-way ANOVA with Tukey post-test for multiple comparison for (H-K) note that statistical difference were not drawn from 6 month data due to low *N* number, $P \leq 0.05$ for *, $P \leq 0.01$ for **, and $P \leq 0.0001$ for ****).

distribution profile at all ages showed that *Smn*$^{2B/-}$;*SMN2*$^{+/-}$ fiber were generally smaller in size as exemplified by a left shift and reduced percentage of large fibers. There was no bi-modal distribution that could suggest concurrent atrophic and hypertrophic fibers in *Smn*$^{2B/-}$;*SMN2*$^{+/-}$ mice (Fig. 3G). In the SMA mice, the atrophic fibers were more numerous, more than double in the female and more than three to four times in the males in comparison to *Smn*$^{2B/+}$;*SMN2*$^{+/-}$ mice (Fig. 3H). In all ages, the atrophic fibers were mostly angulated, characteristic of a denervation etiology. These atrophic fibers were isolated or in groups of two to four (small group atrophy). In rare instances, their number was greater, at times involving a good part of a fascicle (large group atrophy) (data not shown). The atrophy involved both the NADH dense and pale type 2 fibers (data not shown). Overall, we observed a reduced mean fiber size at 12 and 18 months in *Smn*$^{2B/-}$;*SMN2*$^{+/-}$ mice, which appeared independent of sex, but was only significant once male and female were pooled together (Fig. 3I and Supp Fig. 1D). Central nucleation also progressively increased in the muscle over the lifetime of the mice and was worse in male *Smn*$^{2B/-}$;*SMN2*$^{+/-}$ mice (Fig. 3J), suggesting pathological satellite cell activation or muscle immaturity, a feature previously identified in other mouse models of SMA [31]. In fact, many fibers had 2 or more centrally located nuclei, again worse in the male group (Fig. 3K). At all ages, other findings were present but only very infrequently: nuclear grouping, degenerating fibers with or without macrophages, regenerating fibers and, in one sample only (one male at 18 month of age), adipose tissue replacement (data not shown). Altogether, the histological changes suggest a neurogenic atrophy, a finding that appears more severe in male *Smn*$^{2B/-}$;*SMN2*$^{+/-}$ mice.

3.3. Electrophysiological evidence of neurotransmission impairment and NMJ defects in male Smn$^{2B/-}$;SMN2$^{+/-}$ mice

To better understand the neurological and muscular abnormalities in *Smn*$^{2B/-}$;*SMN2*$^{+/-}$ mice, we performed a set of electrophysiological assessments on *ex-vivo* nerve-soleus muscle preparations (Fig. 4A-C). By comparing the force obtained by stimulating first the nerve of the soleus muscle and then the muscle directly (in the presence of tubocurarine to block the neural stimulation at the NMJ), one can identify deficiencies in NMJ transmission. As aging can lead to denervation, young 3–4 month old wild type mice were included as a positive control to show expected values without denervation. Intriguingly, nerve stimulation only generated about 74% of the force generated by direct muscle stimulation in nerve-muscle preparations from male *Smn*$^{2B/-}$;*SMN2*$^{+/-}$ mice (Fig. 4A). Hence, the *Smn*$^{2B/-}$;*SMN2*$^{+/-}$ soleus muscle generated a reduced tetanic force than *Smn*$^{2B/+}$;*SMN2*$^{+/-}$ only when stimulated through the nerve, suggesting a possible disruption of transmission at the NMJ. On the other hand, female *Smn*$^{2B/-}$;*SMN2*$^{+/-}$ mice had relatively spared neurotransmission defects with about 91% of the force generated (Fig. 4A). Both male and female heterozygotes showed minimal sign of defective transmission in comparison to young WT (Fig. 4A). Time to reach peak force was also shorter followed by a small force decrease, mostly in male mice, suggesting that the axons and/or NMJs are unable to maintain neural signaling during a tetanus stimulus
(Fig. 4B-C). This is better depicted by a representative waveform curve from a male *Smn*$^{2B/-}$;*SMN2*$^{+/-}$ mice, which shows a reduced force generation, early force peak and eventual inability to sustain force production when the nerve is stimulated (Fig. 4C). Given that we did not observe any motor neuron loss in our analysis, we wanted to better understand the neurotransmission impairment. We therefore next assessed abnormalities at the NMJ by performing structural analysis of the NMJs and endplates in diaphragm muscle from male *Smn*$^{2B/+}$;*SMN2*$^{+/-}$ and *Smn*$^{2B/-}$;*SMN2*$^{+/-}$ mice. The diaphragm was selected given the complexities in the assessment of the NMJs in skeletal muscle of aged animals and for its properties (thickness and access), as well as the potential respiratory deficits that may be present in aging SMA patients and preclinical models [32]. We observed denervation in about 24% of NMJs, although with some variability (Fig. 4D-J), neurofilament accumulation (Fig. 4K) and disorganized endplates (Fig. 4L). We also investigated whether there was increased ubiquitination, a marker of active muscle atrophy. We observed no difference at 6, 12, or 18 months hindlimb muscle of *Smn*$^{2B/-}$;*SMN2*$^{+/-}$ mice (Fig. 4M-N). This is likely suggesting a very slow and chronic process of muscle atrophy. Overall, these findings confirm a pathologic neuronal/NMJ component.

3.4. Muscle intrinsic contraction/relaxation dynamic defects are present in both male and female Smn$^{2B/-}$;SMN2$^{+/-}$ mice

Other alterations were also readily observed in the muscle component, but this time in both male and female *Smn*$^{2B/-}$;*SMN2*$^{+/-}$ mice. Segregation of males and females showed no difference between sex but highlighted many trends toward defective muscle dynamics (data not shown). Given the low power of analysis with segregated sex and no difference between sex, we decide on combining both males and females together. The contractile component of the tetanic force was relatively preserved as shown by the tetanic force, half rise time and maximum rate of force development (Fig. 5A-C). However, the force-frequency curve of *Smn*$^{2B/+}$;*SMN2*$^{+/-}$ and *Smn*$^{2B/-}$;*SMN2*$^{+/-}$ muscles was shifted to lower stimulation frequency in comparison to muscles from young wild type mice (Fig. 5D). This feature was worse in the *Smn*$^{2B/-}$;*SMN2*$^{+/-}$ mice. Such shift can be due to changes in fiber type composition toward slower fibers or slower relaxation. Prolonged half relaxation time was indeed observed while maximum rate of relaxation showed a trend toward slower dynamics after a tetanic stimulation of either the muscle or the nerve (Fig. 5E-F); an effect also observed with twitch contraction (Fig. 5L-M). Interestingly, while age appears to have an effect on these defects (young wild type vs. *Smn*$^{2B/+}$;*SMN2*$^{+/-}$), it is considerably worse with further SMN depletion as in the *Smn*$^{2B/-}$;*SMN2*$^{+/-}$ mice. Unlike tetanic contraction, there was a trend toward defective components of twitch contraction, such as twitch half-rise time (Fig. 5H) and time to peak (Fig. 5J), while others (twitch force and maximum rate of force development) were not (Fig. 5G, I). Similar relaxation abnormalities as tetanus stimulation were also observed, as exemplified by the slower half relaxation time and maximum relaxation rate, resulting in a wider contraction period (width), which were once again worse in the *Smn*$^{2B/-}$;*SMN2*$^{+/-}$ mice, in comparison to *Smn*$^{2B/+}$;*SMN2*$^{+/-}$ mice (Fig. 5K-M). However, these findings appeared to be unique to muscle stimulation. These results highlight potential deficits in the skeletal muscles.

3.5. Smn$^{2B/-}$;SMN2$^{+/-}$ mice do not display extra-neuronal pathology over time

Extra-neuronal pathology has been described over the past few years in mouse models of SMA. We took advantage of the *Smn*$^{2B/-}$;*SMN2*$^{+/-}$ mice to see whether SMN may be required for cellular maintenance of other organ systems during aging. We first analyzed gross organ size of the heart, spleen, liver, and kidney at 6, 12, 18 and 22 months. No clear and sustained difference was readily apparent over the course of the lifespan (Supp Fig. 2).

We next investigated whether lymphoid organ abnormalities may be present in *Smn*$^{2B/-}$;*SMN2*$^{+/-}$ mice. Three laboratories independently identified small and disorganized spleen in multiple severe mouse models of SMA [30,33-35]. Of note, we did not observe any changes in histology (Supp Fig. 3A-F). We believe that poor perfusion is the reason for the small spleen size in *Smn*$^{2B/-}$ mice (unpublished observations). Interestingly, splenic artery peak systolic velocity and the heart rate remained normal in *Smn*$^{2B/-}$;*SMN2*$^{+/-}$ mice (Supp Fig. 3G-H), thus possibly explaining the normal appearing spleens. More recently, fatty acid metabolism defects were described, where SMA patients were more susceptible to

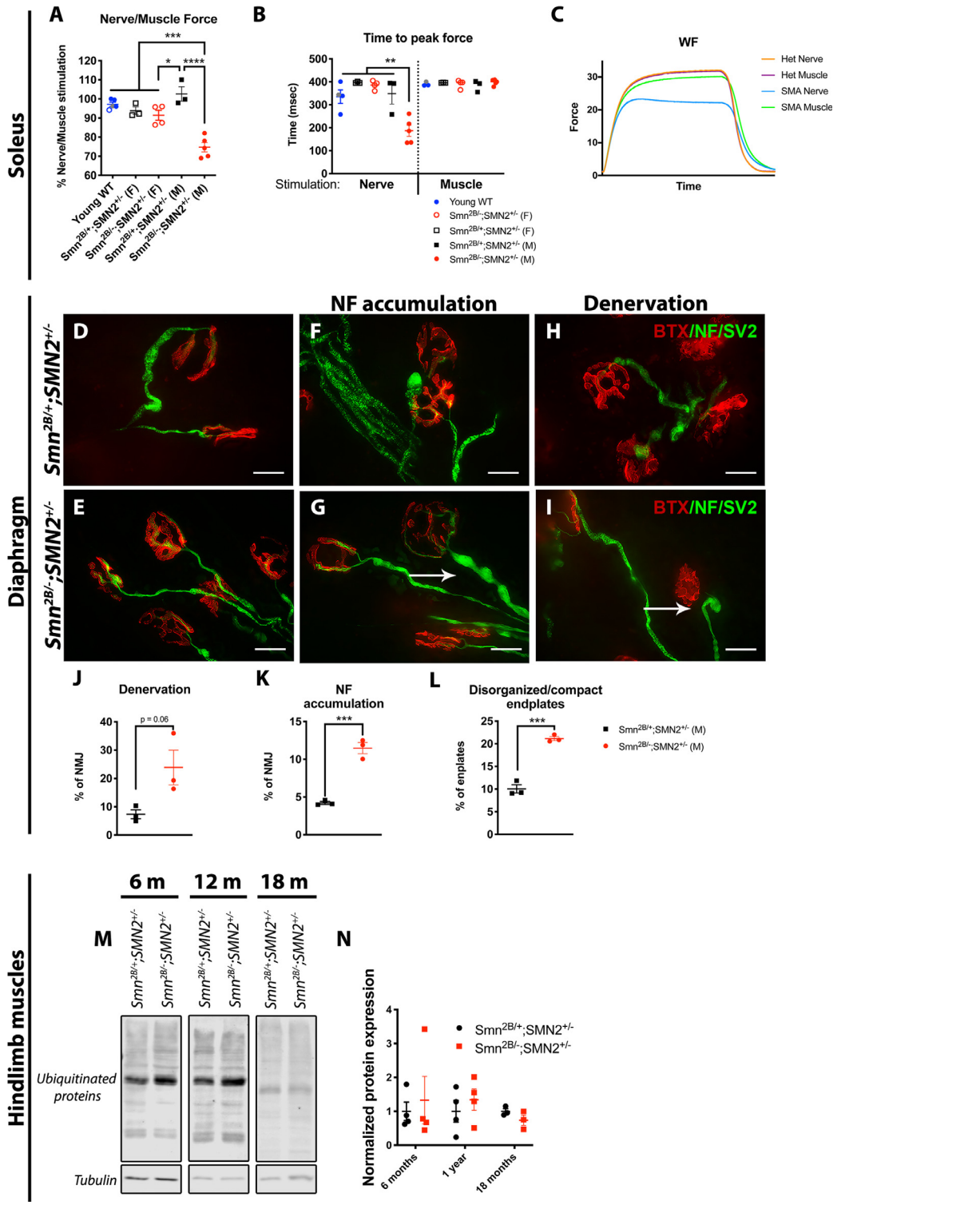

Fig. 4. Impaired neuromuscular transmission and intrinsic muscle relaxation defects at 18 months in *Smn*$^{2B/-}$;*SMN2*$^{+/-}$ mice. (A) Tetanic forces via neural stimulation are expressed as a percent of the tetanic force when solei were directly stimulated. Soleus muscles generated less tetanic force when stimulated via the nerve in male *Smn*$^{2B/-}$;*SMN2*$^{+/-}$ mice (filled in circle), while female *Smn*$^{2B/-}$;*SMN2*$^{+/-}$ mice (hollow circle) were much less affected. This indicates a failure of nerve or NMJ to match the maximum force that can be produced. (B) Peak force occurred sooner in male *Smn*$^{2B/-}$;*SMN2*$^{+/-}$ mice (filled in circle) at 18 months, while female *Smn*$^{2B/-}$;*SMN2*$^{+/-}$ mice (hollow circle) were much less affected, indicating incapacity to sustain neural input by the nerve. (C) Representative waveform of the tetanic force produced by nerve or muscle stimulation in *Smn*$^{2B/-}$;*SMN2*$^{+/-}$ mice (only male depicted). (D-L) Representative images and quantification of diaphragm muscle NMJ staining showing neurofilament accumulation, denervation and disorganized endplates in male *Smn*$^{2B/+}$;*SMN2*$^{+/-}$ and *Smn*$^{2B/-}$;*SMN2*$^{+/-}$ mice. (M-N) Western blot analysis of ubiquitinated proteins in the hindlimb muscle were unchanged in *Smn*$^{2B/-}$;*SMN2*$^{+/-}$ mice. Scale bar represents 20 μm in D-I. The *n* value for each experiment were (A-C) young WT (3–5, 3 males, 1 female and 1 unknown represented in gray), *Smn*$^{2B/+}$;*SMN2*$^{+/-}$ mice (6, 3 females and 3 males), *Smn*$^{2B/-}$;*SMN2*$^{+/-}$ mice (9, 5 males, 4 females); (D-L) $N = 3$ males, (M-N) $N = 3–4$ (undifferentiated for sex). Average ± SEM displayed, (A-C) one-way ANOVA with Tukey post-hoc test, (J-L) unpaired student *t*-test, (N) two-way ANOVA with Tukey post-hoc test, $P \leq 0.05$ for *, $P \leq 0.01$ for **, $P \leq 0.001$ for *** and $P \leq 0.0001$ for ****).

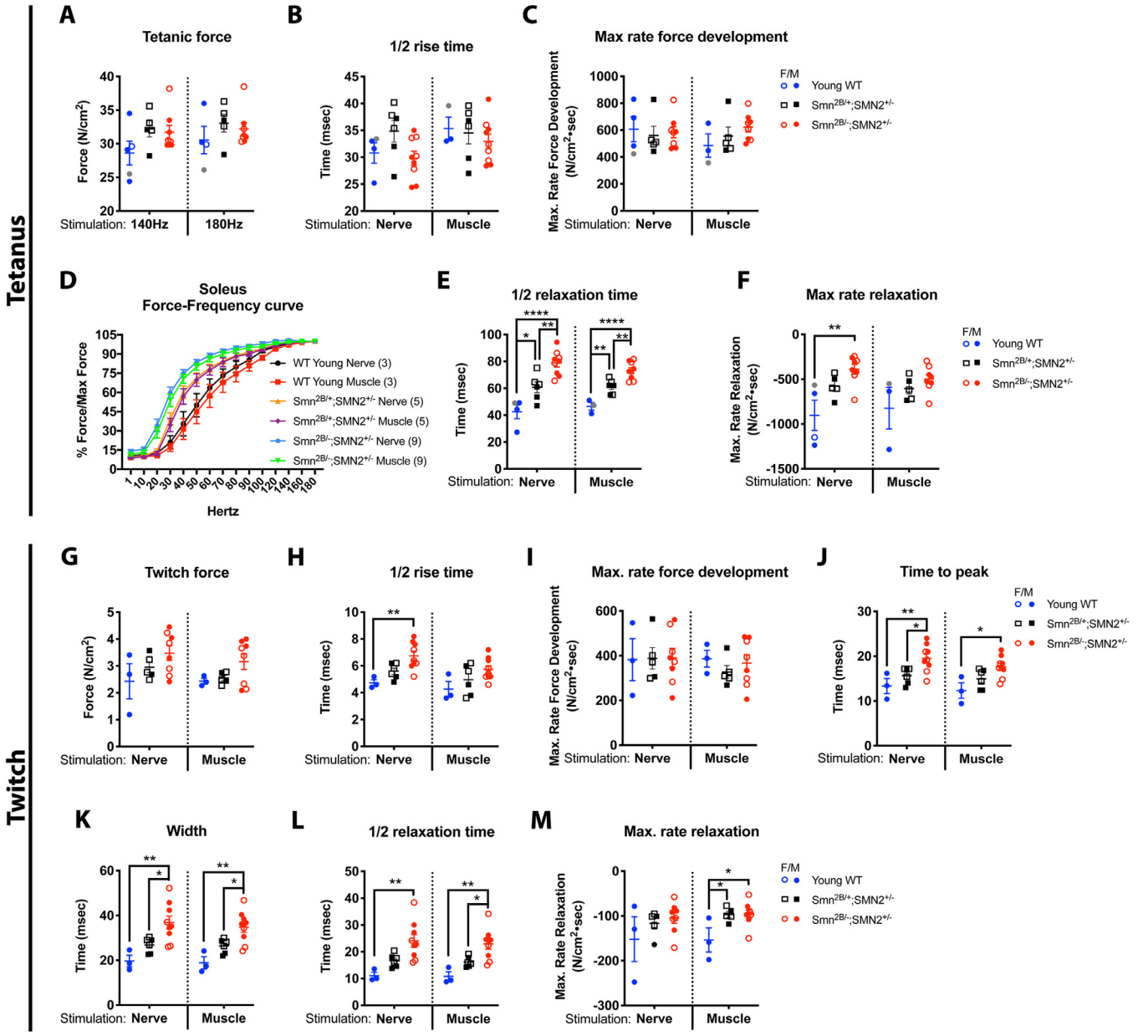

Fig. 5. Impaired muscle relaxation defects at 18 months in *Smn*$^{2B/-}$;*SMN2*$^{+/-}$ mice. (A) tetanic contraction, (B) half rise time, and (C) maximum rate of force development were unaffected in *Smn*$^{2B/-}$;*SMN2*$^{+/-}$ soleus muscle. (D) Force frequency curve of *Smn*$^{2B/-}$;*SMN2*$^{+/-}$ mice was shifted to lower stimulation frequencies possibly linked to slower relaxation. (E-F) Half relaxation time was longer and maximum rate of relaxation trended toward slower dynamics in *Smn*$^{2B/-}$;*SMN2*$^{+/-}$ mice, independent of their sex. Twitch contractions were marked by relatively unchanged force (G), modestly prolonged half rise time (H), unchanged maximum rate of force development (I), increased time to peak (J), increased width (K), increased half relaxation time (L) and a trend toward slower maximum rate of relaxation (M), independent of sex. (The *n* value for each experiment were young WT (3–5, 3 males, 1 female and 1 unknown represented in gray), *Smn*$^{2B/+}$;*SMN2*$^{+/-}$ mice (5–6, 3 females, 3 males), *Smn*$^{2B/-}$;*SMN2*$^{+/-}$ mice (9, 5 males, 4 females). Average ± SEM displayed, one-way ANOVA with Tukey post-hoc test, $P \leq 0.05$ for *, $P \leq 0.01$ for **, and $P \leq 0.0001$ for ****).

dyslipidemia and fatty liver [25] in accordance with initial reports [36-39]. In the *Smn*$^{2B/-}$ mouse model, it led to non-alcoholic fatty liver disease and subsequent functional deficit [25]. *Smn*$^{2B/-}$;*SMN2*$^{+/-}$ livers were unchanged from control and showed no difference in triglycerides and cholesterol esters from 6 to 18 months of age (Supp Fig. 4A-H). Lean mass and fat mass were unchanged at 18 months in the *Smn*$^{2B/-}$;*SMN2*$^{+/-}$ mice (Supp Fig. 4I-J).

Over the past 10 years, a resurgence of case studies has highlighted potential heart defects in severe SMA patients [40]. Similarly, multiple studies of the heart in preclinical models demonstrated bradycardia, reduced function, innervation and vascularization [41-44]. We investigated whether cardiac defects were present in 12 and 18 month old *Smn*$^{2B/-}$;*SMN2*$^{+/-}$ mice using echocardiogram. We found no change in heart rate, stroke volume, cardiac output, ejection fraction and fractional shortening (Supp Fig. 5A-E). These results are in line with a study where no overt cardiac abnormalities were identified in Type II/III patients [45]. As such, it appears that the tail length reduction is not dependent on poor cardiac function but rather subsequent to vasculature issues or dysfunctional neovascularization. Given that no extra-neuronal defects were noted, we did not segregate male and female for further comparison.

4. Discussion

Mild mouse models of SMA have been extremely difficult to generate [8]. As such, pre-clinical modeling of the milder phenotypic

spectrum of the disease, such as type III-IV SMA, and understanding SMN-dependent molecular changes during aging have remained challenging. To fill this gap, we have generated the *Smn*$^{2B/-}$;*SMN2*$^{+/-}$ mouse model, by introducing one allele of *SMN2* to the *Smn*$^{2B/-}$ mice. This additional *SMN2* copy in the *Smn*$^{2B/-}$ mouse background resulted in SMN levels that were slightly elevated than those in the *Smn*$^{2B/-}$ mouse. This subtle increase in SMN was sufficient to lead to a surprising amelioration of the *Smn*$^{2B/-}$ phenotype, yet still showing defects consistent with mild forms of SMA. Note that the level of amelioration may depend on the nature of the *SMN2* transgenic allele utilized. In fact, commonly described *SMN2* alleles can be found at different position in the murine genome, and show varying levels of expression as well as SMN protein production (reviewed in [8]). Additionally, SMN2 single nucleotide changes can also modulate disease as seen in SMA patients [46]. The usage of different *SMN2* alleles compounded to the *Smn*$^{2B/-}$ mice may lead to a varying phenotype that could be leveraged to produce other mouse models in the future.

In comparison to other mouse models of mild SMA (Table 1), the *Smn*$^{2B/-}$;*SMN2*$^{+/-}$ mice display many of the hallmark features that are commonly reported in SMA. These include reduced weight, sustained motor weakness, electrophysiological signs of denervation, NMJ abnormalities and neurogenic muscle atrophy. Other mouse models of mild SMA either show limited features of SMA [16,18,20,22,47,48] or lack potential for aging studies. One study aimed to provide hypomorphic mouse models by the production of mice with increasing SMN2 copy number [20]. This was done by the replacement of murine *Smn* exon 7 and 8 with human *SMN2* exon 7 and 8 (hybrid allele) with or without the addition of varying copy number of the human *SMN2* transgene (genomic human allele) at the murine *Smn* locus [20]. The subsequent breeding of the mice containing the various alleles led to the generation of an allelic series of mice. Unfortunately, the hybrid allele essentially acted as a knock out allele, one copy of human *SMN2* was found to be embryonic lethal and two copies of human *SMN2* (*Smn*$^{C/C}$) seemingly led to a normal lifespan and extremely mild deficits, if any [20]. Yet, the few models that showed promise (SMN$^{RT\ 17}$, A2G *Smn*$^{-/-}$*SMN2* [19], the *Taiwanese* mice (four copies of *SMN2*) [21]), could not be used for aging studies. For example, the A2G *Smn*$^{-/-}$*SMN2* mice display diminished motor neurons, electromyography abnormalities, and muscle atrophy [19]. However, muscle atrophy is identified at 1 month, which may be more closely related to the severe *Smn*$^{2B/-}$ mouse model. Additionally, there was no description of motor function, and progression of the disease [19]. One study made use of antisense oligonucleotides to further reduce SMN levels in the *Taiwanese* model (four copies of *SMN2*) to study SMN function in adulthood [49]. However, this system is unlike the usual SMA pathology given a further reduction in SMN in adulthood (Table 2). Alternatively, others have used low dose of SMN inducing therapy to attain models of milder SMA (Table 2). However, this is more a representation of treated SMA patients rather than the basal SMN levels that an untreated patient would have. To note, we have not seen one classical feature of SMA, namely motor neuron loss, in our *Smn*$^{2B/-}$;*SMN2*$^{+/-}$ mouse model. Recent studies have identified the P53 pathway as the likely culprit whose activation leads to the motor neuron degeneration in SMA [50,51]. Inhibiting the P53 pathway led to an almost complete rescue of motor neurons, but motor deficits, weight and survival were not rescued, highlighting that motor neuron loss is likely a late consequence of disease pathogenesis [51,52]. It is possible that it may simply not be present during a very mild disease course despite clinical motor dysfunction. As such, the *Smn*$^{2B/-}$;*SMN2*$^{+/-}$ mouse represents the first model of mild SMA for studies in adulthood and aging. In this respect, the *Smn*$^{2B/-}$;*SMN2*$^{+/-}$ mice provide many benefits. They allow study of the earliest and perhaps most susceptible molecular changes that occur with SMN depletion. They will also permit long experimental paradigms such as muscle regeneration after cardiotoxin treatment, diet modulation, and exercise. With the addition of a *SMN2* allele, the need for sustained splicing modulators (in the case of Spinraza) in mild SMA can be trialed in these mice. This could be very informative for current adult patients with established SMA pathology.

Our characterization of the *Smn*$^{2B/-}$;*SMN2*$^{+/-}$ mice revealed some surprising findings. First, the electrophysiological data showed selective preferential transmission/denervation defects in the male mice, with the female mice showing almost no deficiencies in these measurements. In male *Smn*$^{2B/-}$;*SMN2*$^{+/-}$ mice, neuronal stimulation could only reach about 74% of the tetanic force generated by stimulating the muscle directly, implying that 26% of the fibers do not get recruited by neurons. The inability to sustain tetanic contraction in male vs. female *Smn*$^{2B/-}$;*SMN2*$^{+/-}$ mice, as shown by the time to peak force was striking. This feature is not reproduced by muscle stimulation, thereby eliminating a possible muscle etiology and confirming that the localization of the defect lies at the axon or the NMJ. It should be noted that the electrophysiological experimental paradigm used in this study does not allow us to distinguish between a conduction block within the nerve or a deficient process at the NMJ in the inability to sustain tetanic contraction. A nerve conduction study would help differentiate alterations in axonal conduction or failure at the NMJ. Similarly, the prominence of centrally located nuclei was also more pronounced in the male *Smn*$^{2B/-}$;*SMN2*$^{+/-}$ mice. The link, if any, between reduced neurotransmission and central nucleation remains unknown. Nevertheless, it is not the first time that sex differences are brought up in the context of SMA. The preferential severity to the male population is in line with the majority of clinical reports discussing sex differences, particularly in milder types of SMA [53-56]. Some studies highlight a lower incidence of disease onset after female puberty and subsequently a predominance of males in the mild SMA types [56-58]. Furthermore, females appear over-represented in the asymptomatic biallelic *SMN1* deletion carrier population [53,55,57,59-62]. This may be related to genetic modifiers, such as plastin 3, that appear to be female sex dependent [63,64]. Most recently, a drug cessation study also showed that male mice may be more susceptible to SMN depletion in a therapeutic context (Chien-Ping Ko, personal communication, CureSMA poster presentation 2017). Nevertheless, the scientific literature on sex differences in SMA remains relatively sparse. While some features were more predominant in males in our study, not all findings display a sex-dependent difference. For example, most histological changes (apart from central nucleation) and the electrophysiological muscle defects were not dependent on the sex of the mice. The exact mechanism for this sex difference remains unclear. The female and male comparison of the *Smn*$^{2B/-}$;*SMN2* mice could yield new genetic modifiers with therapeutic potential. Altogether, these findings strongly highlight the importance of considering sex in pre-clinical and clinical experimental framework.

Another interesting but unexpected feature of the *Smn*$^{2B/-}$;*SMN2*$^{+/-}$ mice was the emergence of potential intrinsic muscle defects. This is first evidenced by the sustained increase in the proportion of centrally located nuclei in skeletal muscle, which appears more severe than the unspecific central nucleation that is consequence from denervation. In our experimental scheme, it is possible that the increased central nucleation in the muscle of *Smn*$^{2B/-}$;*SMN2*$^{+/-}$ mice is a sign of constant satellite cell activation or regeneration, highlighting a possible compensatory mechanism or abnormal satellite cell function. Interestingly, we have previously identified increased central nucleation in *Smn*$^{2B/-}$ and *Smn*$^{-/-}$;*SMN2*$^{+/-}$ mice despite the absence of degenerating fibers [31], both representing severe models of SMA. Furthermore, the appearance of a myopathy was also described in mice where inducible SMN depletion was performed in adulthood [65]. However, the studies reported for this latter model extended only until 9 months of age, giving limited information about aged SMN-depleted muscle and motor neurons [65]. In accordance with our findings, a recent study with specific SMN depletion in muscle lead to motor deficits, increased centrally located nuclei, deficit in muscle regeneration and NMJ defects [66]. Future thorough assessment of muscle regeneration in tandem with

in vitro isolation of satellite cells during aging in mild SMA mice will be required to understand SMN involvement, if any, in satellite cell biology. Furthermore, the electrophysiological data we present also revealed some potential relaxation defects in both the tetanus and twitch stimulation (half relaxation time, maximum rate of relaxation, width) regardless of receiving stimulation through the nerve or the muscle. In contrast to the defect in NMJ/neuronal transmission, the muscle defects appear to be similar amongst male and female *Smn*$^{2B/-}$;*SMN2*$^{+/-}$ mice. Of importance, the overall capacity to generate force was not affected when normalized on muscle weight and length, meaning that muscle intrinsic weakness is unlikely to contribute to the motor impairment seen in this mild model. This is in contrast with more severe SMA models [67]. One of the pitfalls of our experimental paradigm lies in the different muscles used for different experiments (TA in histological assessment and soleus in electrophysiological assessment), which are muscles that have different fiber type composition. Unfortunately, this is unavoidable due to the difficulty in using the TA for electrophysiological experiments. Nevertheless, it is possible that different muscles have pathologic heterogeneity as previously shown in the context of SMA [68]. Despite this, our results further stress probable SMN-dependent muscle intrinsic defects.

While direct comparison to human SMA is difficult, the *Smn*$^{2B/-}$;*SMN2*$^{+/-}$ mice more closely represents the mild type III or type IV SMA patients. Literature on type IV SMA patients is extremely sparse and date prior to genetic studies [69]. Their symptomatology is usually extremely slow (i.e., over 20 years course), marked by gradual fasciculations and mild progressive weakness which may eventually lead to the patient becoming wheelchair bound or requiring assistance with walking [69]. In the new era of SMA treatment, it remains unclear whether persistent interventions will be required, and long-term complete reversal of symptoms will be attained. Therefore, it is likely that type I SMA patients will transition into a less severe type III-IV once treated, giving them a longer or normal lifespan. There is a paucity of studies investigating the support and medical needs of type IV SMA patients (and soon the treated patients) as they age. Ideally, one would want to limit comorbidities that may arise naturally or upon challenges. In recent years, the SMA field has witnessed a surge in the identification of extra-neuronal defects, mostly in pre-clinical models and less often in humans (reviewed in [70]). With some reassurance, according to the model studied here, the spleen, the liver and heart remain unaffected.

Altogether, the *Smn*$^{2B/-}$;*SMN2*$^{+/-}$ mouse model provides an adequate, and most thoroughly described, model of mild SMA. It will allow investigation of the most susceptible defects that arise with SMN-depletion, particularly in aging. Furthermore, this model will confer anticipatory guidance of treated SMA patients that are likely to age far beyond SMA natural history.

Declaration of Competing Interest

Marc-Olivier Deguise received honoraria and travel accommodations by Biogen for the SMA Summit 2018 held in Montreal, Canada and the SMA Academy 2019 held in Toronto, Canada. Rashmi Kothary and the Ottawa Hospital Research Institute have a licensing agreement with Biogen for the *Smn*$^{2B/-}$ mouse model. These COI are outside the scope of this study. All other authors have no competing interests to declare.

Acknowledgments

We would like to thank My Tran Trung, the histological core, behavioral core and the pre-clinical imaging core (Gregory Cron) of the University of Ottawa, as well as Frederick R. Roberts from FujiFilm VisualSonics and Harry Coenraad from the pathology department of the Children's Hospital of Eastern Ontario for assistance with experiments. We would like to thank all members of the Kothary laboratory for helpful discussions.

Funding

This work was supported by Cure SMA/Families of SMA Canada (Grant number KOT-1819 and KOT-2021); Muscular Dystrophy Association Inc. (USA) (Grant number 575466); and Canadian Institutes of Health Research (CIHR) (Grant number PJT-156379). M-O.D was supported by a Frederick Banting and Charles Best CIHR Doctoral Research Award and LC is supported by an Ontario Graduate Scholarship Award.

Supplementary materials

Supplementary material associated with this article can be found in the online version at doi:10.1016/j.ebiom.2020.102750.

References

[1] Lefebvre S, Burglen L, Reboullet S, et al. Identification and characterization of a spinal muscular atrophy- determining gene. Cell 1995;80(1):155–65.
[2] Verhaart IEC, Robertson A, Wilson IJ, et al. Prevalence, incidence and carrier frequency of 5q-linked spinal muscular atrophy - a literature review. Orphanet J Rare Dis 2017;12(1):124.
[3] Feldkotter M, Schwarzer V, Wirth R, Wienker TF, Wirth B. Quantitative analyses of SMN1 and SMN2 based on real-time lightCycler PCR: fast and highly reliable carrier testing and prediction of severity of spinal muscular atrophy. Am J Hum Genet 2002;70(2):358–68.
[4] Oskoui M, Darras B, De Vivo D. Spinal muscular atrophy: 125 years later and on the verge of a cure. In: Sumner CJ, Paushkin S, Ko CP, editors. Spinal muscular atrophy: disease mechanisms and therapy. 1st ed. Academic Press and Elsevier; 2017. p. 3–19.
[5] Finkel RS, Chiriboga CA, Vajsar J, et al. Treatment of infantile-onset spinal muscular atrophy with nusinersen: a phase 2, open-label, dose-escalation study. Lancet 2016;388(10063):3017–26.
[6] Finkel RS, Mercuri E, Darras BT, et al. Nusinersen versus sham control in infantile-onset spinal muscular atrophy. N Engl J Med 2017;377(18):1723–32.
[7] Mendell JR, Al-Zaidy S, Shell R, et al. Single-dose gene-replacement therapy for spinal muscular atrophy. N Engl J Med 2017;377(18):1713–22.
[8] Burghes AH, DiDonato CJ, McGivern JV, Arnold WD. Mammalian models of spinal muscular atrophy. In: Sumner CJ, Paushkin S, Ko CP, editors. Spinal muscular atrophy: disease mechanisms and therapy. Academic Press and Elsevier; 2017. p. 241–60.
[9] Hsieh-Li HM, Chang JG, Jong YJ, et al. A mouse model for spinal muscular atrophy. Nat Genet 2000;24(1):66–70.
[10] Le TT, Pham LT, Butchbach ME, et al. SMNDelta7, the major product of the centromeric survival motor neuron (SMN2) gene, extends survival in mice with spinal muscular atrophy and associates with full-length SMN. Hum Mol Genet 2005;14(6):845–57.
[11] Monani UR, Sendtner M, Coovert DD, et al. The human centromeric survival motor neuron gene (SMN2) rescues embryonic lethality in Smn(-/-) mice and results in a mouse with spinal muscular atrophy. Hum Mol Genet 2000;9(3):333–9.
[12] Bowerman M, Murray LM, Beauvais A, Pinheiro B, Kothary R. A critical SMN threshold in mice dictates onset of an intermediate spinal muscular atrophy phenotype associated with a distinct neuromuscular junction pathology. Neuromuscul Disord 2012;22(3):263–76.
[13] DiDonato CJ, Lorson CL, De Repentigny Y, et al. Regulation of murine survival motor neuron (Smn) protein levels by modifying Smn exon 7 splicing. Hum Mol Genet 2001;10(23):2727–36.
[14] Hammond SM, Gogliotti RG, Rao V, Beauvais A, Kothary R, DiDonato CJ. Mouse survival motor neuron alleles that mimic SMN2 splicing and are inducible rescue embryonic lethality early in development but not late. PLoS ONE 2010;5(12):e15887.
[15] Eshraghi M, McFall E, Gibeault S, Kothary R. Effect of genetic background on the phenotype of the Smn2B/- mouse model of spinal muscular atrophy. Hum Mol Genet 2016;25(20):4494–506.
[16] Bogdanik LP, Osborne MA, Davis C, et al. Systemic, postsymptomatic antisense oligonucleotide rescues motor unit maturation delay in a new mouse model for type II/III spinal muscular atrophy. Proc Natl Acad Sci U S A 2015;112(43):E5863–72.
[17] Cobb MS, Rose FF, Rindt H, et al. Development and characterization of an SMN2-based intermediate mouse model of spinal muscular atrophy. Hum Mol Genet 2013;22(9):1843–55.
[18] Gladman JT, Bebee TW, Edwards C, et al. A humanized Smn gene containing the SMN2 nucleotide alteration in exon 7 mimics SMN2 splicing and the SMA disease phenotype. Hum Mol Genet 2010;19(21):4239–52.
[19] Monani UR, Pastore MT, Gavrilina TO, et al. A transgene carrying an A2G missense mutation in the SMN gene modulates phenotypic severity in mice with severe (type I) spinal muscular atrophy. J Cell Biol 2003;160(1):41–52.
[20] Osborne M, Gomez D, Feng Z, et al. Characterization of behavioral and neuromuscular junction phenotypes in a novel allelic series of SMA mouse models. Hum Mol Genet 2012;21(20):4431–47.
[21] Tsai LK, Tsai MS, Lin TB, Hwu WL, Li H. Establishing a standardized therapeutic testing protocol for spinal muscular atrophy. Neurobiol Dis 2006;24(2):286–95.

[22] Workman E, Saieva L, Carrel TL, et al. A SMN missense mutation complements SMN2 restoring snRNPs and rescuing SMA mice. Hum Mol Genet 2009;18(12):2215–29.
[23] Gogliotti RG, Lutz C, Jorgensen M, Huebsch K, Koh S, Didonato CJ. Characterization of a commonly used mouse model of SMA reveals increased seizure susceptibility and heightened fear response in FVB/N mice. Neurobiol Dis 2011;43(1):142–51.
[24] Shafey D, Boyer JG, Bhanot K, Kothary R. Identification of novel interacting protein partners of SMN using tandem affinity purification. J Proteome Res 2010;9(4):1659–69.
[25] Deguise MO, Baranello G, Mastella C, et al. Abnormal fatty acid metabolism is a core component of spinal muscular atrophy. Ann Clin Transl Neurol 2019;6(8):1519–32.
[26] Folch J, Lees M, Sloane Stanley GH. A simple method for the isolation and purification of total lipides from animal tissues. J Biol Chem 1957;226(1):497–509.
[27] Morrison WR, Smith LM. Preparation of fatty acid methyl esters and dimethylacetals from lipids with boron fluoride–methanol. J Lipid Res 1964;5:600–8.
[28] Gong B, Legault D, Miki T, Seino S, Renaud JM. KATP channels depress force by reducing action potential amplitude in mouse EDL and soleus muscle. Am J Physiol Cell Physiol 2003;285(6):C1464–74.
[29] Hua Y, Sahashi K, Rigo F, et al. Peripheral SMN restoration is essential for long-term rescue of a severe spinal muscular atrophy mouse model. Nature 2011;478(7367):123–6.
[30] Deguise MO, De Repentigny Y, McFall E, Auclair N, Sad S, Kothary R. Immune dysregulation may contribute to disease pathogenesis in spinal muscular atrophy mice. Hum Mol Genet 2017;26(4):801–19.
[31] Boyer JG, Deguise MO, Murray LM, et al. Myogenic program dysregulation is contributory to disease pathogenesis in spinal muscular atrophy. Hum Mol Genet 2014;23(16):4249–59.
[32] Neve A, Trub J, Saxena S, Schumperli D. Central and peripheral defects in motor units of the diaphragm of spinal muscular atrophy mice. Mol Cell Neurosci 2016;70:30–41.
[33] Deguise MO, Kothary R. New insights into SMA pathogenesis: immune dysfunction and neuroinflammation. Ann Clin Transl Neurol 2017;4(7):522–30.
[34] Khairallah MT, Astroski J, Custer SK, Androphy EJ, Franklin CL, Lorson CL. SMN deficiency negatively impacts red pulp macrophages and spleen development in mouse models of spinal muscular atrophy. Hum Mol Genet 2017;26(5):932–41.
[35] Thomson AK, Somers E, Powis RA, et al. Survival of motor neurone protein is required for normal postnatal development of the spleen. J Anat 2017;230(2):337–46.
[36] Crawford TO, Sladky JT, Hurko O, Besner-Johnston A, Kelley RI. Abnormal fatty acid metabolism in childhood spinal muscular atrophy. Ann Neurol 1999;45(3):337–43.
[37] Tein I, Sloane AE, Donner EJ, Lehotay DC, Millington DS, Kelley RI. Fatty acid oxidation abnormalities in childhood-onset spinal muscular atrophy: primary or secondary defect(s)? Pediatr Neurol 1995;12(1):21–30.
[38] Zolkipli Z, Sherlock M, Biggar WD, et al. Abnormal fatty acid metabolism in spinal muscular atrophy may predispose to perioperative risks. Eur J Paediatr Neurol 2012;16(5):549–53.
[39] Kelley RI, Sladky JT. Dicarboxylic aciduria in an infant with spinal muscular atrophy. Ann Neurol 1986;20(6):734–6.
[40] Rudnik-Schoneborn S, Heller R, Berg C, et al. Congenital heart disease is a feature of severe infantile spinal muscular atrophy. J Med Genet 2008;45(10):635–8.
[41] Bevan AK, Hutchinson KR, Foust KD, et al. Early heart failure in the SMNDelta7 model of spinal muscular atrophy and correction by postnatal scAAV9-SMN delivery. Hum Mol Genet 2010;19(20):3895–905.
[42] Heier CR, Satta R, Lutz C, DiDonato CJ. Arrhythmia and cardiac defects are a feature of spinal muscular atrophy model mice. Hum Mol Genet 2010;19(20):3906–18.
[43] Shababi M, Habibi J, Ma L, Glascock JJ, Sowers JR, Lorson CL. Partial restoration of cardio-vascular defects in a rescued severe model of spinal muscular atrophy. J Mol Cell Cardiol 2012;52(5):1074–82.
[44] Shababi M, Habibi J, Yang HT, Vale SM, Sewell WA, Lorson CL. Cardiac defects contribute to the pathology of spinal muscular atrophy models. Hum Mol Genet 2010;19(20):4059–71.
[45] Palladino A, Passamano L, Taglia A, et al. Cardiac involvement in patients with spinal muscular atrophies. Acta Myol 2011;30(3):175–8.
[46] Prior TW, Krainer AR, Hua Y, et al. A positive modifier of spinal muscular atrophy in the SMN2 gene. Am J Hum Genet 2009;85(3):408–13.
[47] Jablonka S, Schrank B, Kralewski M, Rossoll W, Sendtner M. Reduced survival motor neuron (Smn) gene dose in mice leads to motor neuron degeneration: an animal model for spinal muscular atrophy type III. Hum Mol Genet 2000;9(3):341–6.
[48] Simon CM, Jablonka S, Ruiz R, Tabares L, Sendtner M. Ciliary neurotrophic factor-induced sprouting preserves motor function in a mouse model of mild spinal muscular atrophy. Hum Mol Genet 2010;19(6):973–86.
[49] Sahashi K, Ling KK, Hua Y, et al. Pathological impact of SMN2 mis-splicing in adult SMA mice. EMBO Mol Med 2013;5(10):1586–601.
[50] Murray LM, Beauvais A, Gibeault S, Courtney NL, Kothary R. Transcriptional profiling of differentially vulnerable motor neurons at pre-symptomatic stage in the Smn (2b/-) mouse model of spinal muscular atrophy. Acta Neuropathol Commun 2015;3:55.
[51] Simon CM, Dai Y, Van Alstyne M, et al. Converging mechanisms of p53 activation drive motor neuron degeneration in spinal muscular atrophy. Cell Rep 2017;21(13):3767–80.
[52] Courtney NL, Mole AJ, Thomson AK, Murray LM. Reduced P53 levels ameliorate neuromuscular junction loss without affecting motor neuron pathology in a mouse model of spinal muscular atrophy. Cell Death Dis 2019;10(7):515.
[53] Capon F, Levato C, Merlini L, et al. Discordant clinical outcome in type iii spinal muscular atrophy sibships showing the same deletion pattern. Neuromuscul Disord 1996;6(4):261–4.
[54] Furukawa T, Nakao K, Sugita H, Tsukagoshi H. Kugelberg-Welander disease with particular reference to sex-influenced manifestations. Arch Neurol 1968;19(2):156–62.
[55] Hahnen E, Forkert R, Marke C, et al. Molecular analysis of candidate genes on chromosome 5q13 in autosomal recessive spinal muscular atrophy: evidence of homozygous deletions of the SMN gene in unaffected individuals. Hum Mol Genet 1995;4(10):1927–33.
[56] Hausmanowa-Petrusewicz I, Zaremba J, Borkowska J. Chronic proximal spinal muscular atrophy of childhood and adolescence: problems of classification and genetic counselling. J Med Genet 1985;22(5):350–3.
[57] Jedrzejowska M, Milewski M, Zimowski J, et al. Phenotype modifiers of spinal muscular atrophy: the number of SMN2 gene copies, deletion in the NAIP gene and probably gender influence the course of the disease. Acta Biochim Pol 2009;56(1):103–8.
[58] Zerres K, Rudnik-Schoneborn S. Natural history in proximal spinal muscular atrophy. Clinical analysis of 445 patients and suggestions for a modification of existing classifications. Arch Neurol 1995;52(5):518–23.
[59] Helmken C, Hofmann Y, Schoenen F, et al. Evidence for a modifying pathway in SMA discordant families: reduced SMN level decreases the amount of its interacting partners and Htra2-beta1. Hum Genet 2003;114(1):11–21.
[60] Cobben JM, van der Steege G, Grootscholten P, de Visser M, Scheffer H, Buys CH. Deletions of the survival motor neuron gene in unaffected siblings of patients with spinal muscular atrophy. Am J Hum Genet 1995;57(4):805–8.
[61] Cusco I, Barcelo MJ, Rojas-Garcia R, et al. SMN2 copy number predicts acute or chronic spinal muscular atrophy but does not account for intrafamilial variability in siblings. J Neurol 2006;253(1):21–5.
[62] Wang CH, Xu J, Carter TA, et al. Characterization of survival motor neuron (SMNT) gene deletions in asymptomatic carriers of spinal muscular atrophy. Hum Mol Genet 1996;5(3):359–65.
[63] Oprea GE, Krober S, McWhorter ML, et al. Plastin 3 is a protective modifier of autosomal recessive spinal muscular atrophy. Science 2008;320(5875):524–7.
[64] Stratigopoulos G, Lanzano P, Deng L, et al. Association of plastin 3 expression with disease severity in spinal muscular atrophy only in postpubertal females. Arch Neurol 2010;67(10):1252–6.
[65] Kariya S, Obis T, Garone C, et al. Requirement of enhanced survival motoneuron protein imposed during neuromuscular junction maturation. J Clin Invest 2014;124(2):785–800.
[66] Kim JK, Jha NN, Feng Z, et al. Muscle-specific SMN reduction reveals motor neuron-independent disease in spinal muscular atrophy models. J Clin Invest 2020.
[67] Boyer JG, Murray LM, Scott K, De Repentigny Y, Renaud JM, Kothary R. Early onset muscle weakness and disruption of muscle proteins in mouse models of spinal muscular atrophy. Skelet Muscle 2013;3(1):24.
[68] Kong L, Wang X, Choe DW, et al. Impaired synaptic vesicle release and immaturity of neuromuscular junctions in spinal muscular atrophy mice. J Neurosci 2009;29(3):842–51.
[69] Pearn JH, Hudgson P, Walton JN. A clinical and genetic study of spinal muscular atrophy of adult onset: the autosomal recessive form as a discrete disease entity. Brain 1978;101(4):591–606.
[70] Deguise MO, Patitucci TN, Ebert AD, Lorson CL, Kothary R. Contributions of different cell types to spinal muscular atrophy pathogenesis. In: Sumner CJ, Paushkin S, Ko CP, editors. Spinal muscular atrophy: disease mechanisms and therapy. Academic Press; 2017. p. 167–90.
[71] Zhou H, Meng J, Marrosu E, Janghra N, Morgan J, Muntoni F. Repeated low doses of morpholino antisense oligomer: an intermediate mouse model of spinal muscular atrophy to explore the window of therapeutic response. Hum Mol Genet 2015;24(22):6265–77.
[72] Feng Z, Ling KK, Zhao X, et al. Pharmacologically induced mouse model of adult spinal muscular atrophy to evaluate effectiveness of therapeutics after disease onset. Hum Mol Genet 2016;25(5):964–75.
[73] Long KK, O'Shea KM, Khairallah RJ, et al. Specific inhibition of myostatin activation is beneficial in mouse models of SMA therapy. Hum Mol Genet 2019;28(7):1076–89.